Contrib Mineral Petrol (2010) 160:219–238
DOI 10.1007/s00410-009-0474-6

ORIGINAL PAPER

The effect of different second-phase particle regimes on grain growth in two-phase aggregates: insights from in situ rock analogue experiments

Sabine Helene Brodhag · Marco Herwegh

Received: 14 January 2009 / Accepted: 26 November 2009 / Published online: 24 December 2009

Abstract The aim of the study was to investigate the effect of rigid second phases on grain growth of a matrix phase. For this purpose, variable mixtures of norcamphor as the matrix phase, with glass beads (0.08–0.51 volume fraction) as second phase, were used to perform see-through rock-analogue experiments under static conditions at constant temperatures (50°C). Irrespective of the second-phase content, grain-size evolution of all mixtures can be subdivided into a stage of continuous grain growth, a transient stage and a stage of a finally stabilized grain size. On the grain-scale, the second phases affect the migrating grain boundaries either by pinning by single particles, by multiple particles or even by particle clusters. Summed up over the entire aggregate, these pinning regimes affect the average bulk grain size of the matrix grains, such that the changes in matrix grain size directly correlate with the amount of second phases, their dispersion and their degree of clustering. In this way, the matrix grain size decreases with increasing second-phase content, which can be expressed as a Zener relationship. Originating from the modification of an ordinary grain growth law, a new mathematical expression is defined, which allows the calculation of changes in the matrix grain size as a function of different second-phase volume fractions and particle sizes. Such models will be helpful in the future to predict microstructural changes in polymineralic rocks at depth.

Keywords Static grain growth · Second phases · Zener pinning · Analogue experiment · Norcamphor · Growth law · Calcite · Pinning regimes

Communicated by J. Hoefs.

Electronic supplementary material The online version of this article (doi:10.1007/s00410-009-0474-6) contains supplementary material, which is available to authorized users.

S. H. Brodhag (✉) · M. Herwegh
Institute of Geological Sciences, University of Bern, Bern, Switzerland
e-mail: brodhag@geo.unibe.ch

Introduction

Static grain growth is one of the most fundamental metamorphic processes in the Earth's crust and mantle (Joesten 1991) occurring in almost every rock. Profound knowledge on the processes and kinetics of grain growth are important because grain growth affects the size, shape and crystallographic orientation of mineral grains, and therefore, also the rock's physical properties, such as viscous and brittle strength (Brook 1976; Olgaard and Evans 1988). Furthermore, changes in grain size directly influence the grain boundary network, which controls diffusion and mass transfer due to decreasing grain boundary volume and consequently lower permeability. This has important implications for metamorphic petrology, where grain boundaries often act as preferential pathways for mass transfer (e.g. Carlson and Gordon 2004). To understand the processes of grain growth, numerous studies in monomineralic rocks have been carried out for most common mineral systems (calcite: Covey-Crump 1996; Berger and Herwegh 2004; Ebert, et al. 2007; calcite, quartz: Tullis and Yund 1982; olivine: Karato 1989; Faul and Scott 2006; anorthite: Dresen et al. 1996; rocksalt: Bestmann et al. 2005) and equivalent rock analogue materials (norcamphor and OCP: Bons et al. 2000; Park et al. 2001; norcamphor and benzamide: Rosenberg and Handy 2001; octachloropropane: Means 1983; Nam et al. 1999; sodium nitrate: Haggert et al. 1992; alum: Nollet et al. 2006; halite: Schenk et al. 2006).

Based on the aforementioned experiments, four stages of grain-size evolution can be distinguished (Andrade and Aboav 1966; Simpson, et al. 1971; Olgaard and Evans 1988): a first stage (I) comprises densification of the aggregate and the processes of initial recrystallization, in which specifically the combination of internally stored strain and surface energy of a grain represent the driving forces during fast grain growth (see Fig. 1 in Olgaard and Evans 1988). A constant rate of normal grain growth characterizes stage II, in which grain boundary migration is mainly driven by a reduction of the grain's surface energy. Next, a reduction in grain boundary migration due to the presence of chemical impurities (e.g. solute atoms) or second phases (e.g. pores, second-phase minerals) defines the onset of stage III (see Fig. 9 in Covey-Crump and Rutter 1989), which can even lead to a complete immobilization of grain boundaries and therefore, to a finally stabilized grain size (stage IV).

In nature, almost all rocks are polymineralic or contain chemical impurities. In rocks consisting of a predominant matrix phase (volume fraction (f_p) > 0.5) additional minerals present are referred to as second phases ($f_p < 0.5$). The presence of such second phases affects grain growth of the matrix phase: it retards and impedes grain growth and constrains or even pins the migration of grain boundaries. Therefore, type, amount, dispersion, and physical properties of second phases determine grain growth and the physical properties of a rock. Initially, research on grain growth behaviour and grain scale processes was experimentally conducted in the field of material sciences on monomineralic metals (e.g., Andrade and Aboav 1966; Simpson et al. 1971) as well as on two-phase metallic systems and alloys (Smith 1948; Dai et al. 1999; Ferry et al. 2005). Meanwhile, experimental approaches are expanded by numerical modelling (Jessell et al. 2001, 2003; Solomatov et al. 2002; Moelans et al. 2005; El-Khozondar et al. 2006; Zheng et al. 2006; Becker et al. 2008). In industrial applications, micro- to nano-scale grain sizes are important for superior physical and mechanical properties of high-quality materials and, thus, pinning of the matrix grains by second-phase particles is an effective tool to control the grain growth process and the final grain size of the aggregate (Andersen and Grong 1994; Manohar et al. 1998).

On the basis of a series of rock analogue experiments with variable volume fractions of second phases, we investigate the effect of second-phase particles on static grain growth of the matrix phase. In the second part of this contribution, the new results are used to develop a mathematical model for grain growth in second-phase affected systems, the relevance of which is discussed for nature.

Experimental setup and method

Norcamphor ($C_7H_{10}O$, bicyclo[2.2.1]heptan-2-one) is a well-approved rock analogue material to quartz (Bons 1993; Herwegh and Handy 1996, 1998; Bauer et al. 2000b; Walte et al. 2005, 2007) showing uniaxial negative optical properties. It consists of soft, beige-coloured crystals and has a melting point around 367 K (Bons 1993), which can be decreased in the presence of additional water (Bauer et al. 2000a). Due to the molecular crystal structure (Bons 1993) it serves as an H-bond acceptor (data sheet of Sigma–Aldrich) inducing a weak polar behaviour.

In situ experiments with norcamphor have the advantage of simple handling, as they can be performed at relatively low-temperature conditions, and the microstructural evolution can be continuously monitored under the microscope (e.g., Herwegh et al. 1997). This approach allows the correlation between processes and microstructures observed in experiments and nature. In addition to the norcamphor phase, we used micro glass beads as a second phase to investigate static grain growth of the matrix phase in polymineralic aggregates. The glass beads are characterized by spherical shapes and particle sizes (d_p) between 70 and 100 μm. They represent a rigid, equiaxed and non-reacting second-phase material leading to a reduction of complexity of our polymineralic systems and, therefore, allow focusing on the microstructural evolution of the matrix phase only. Several experiments with different volume fractions (f_p) of glass beads were performed to observe the norcamphor grain growth in direct subjection to the second-phase volume fraction (Fig. 1).

Sample preparation was performed following Herwegh and Handy (1996). Depending on the required volume fraction of second phases, glass beads with the corresponding weight fraction were mixed with the correlating amount of norcamphor powder. The mixture was cold pressed to platelets of about 140–400 μm thickness (Table 1), cut, remixed and cold pressed again. This cycle was repeated up to three times to guarantee a good mixture between matrix and second phase, as well as a suitable dispersion of second-phase particles. The pressed norcamphor slice was mounted between two glass plates, which were sealed together with instant cyanoacrylic-based adhesive to prevent sublimation of norcamphor. The sample assembly was placed in a heated Urai-Means rock-analogue rig (see Fig. 1 in Herwegh and Handy 1996), which was mounted underneath a modified Wild Macroscope. The Wild Macroscope was equipped with a SONY DW-F-X 700 camera and the automatic rotation polarizing system of Fueten (1997). In combination with the modified Macroscope, the free software package GeoVision (GV) of Fueten (http://Spartan.ac.brocku.ca/~fueten/stage/Download/DownloadF.html) was used to capture automatically

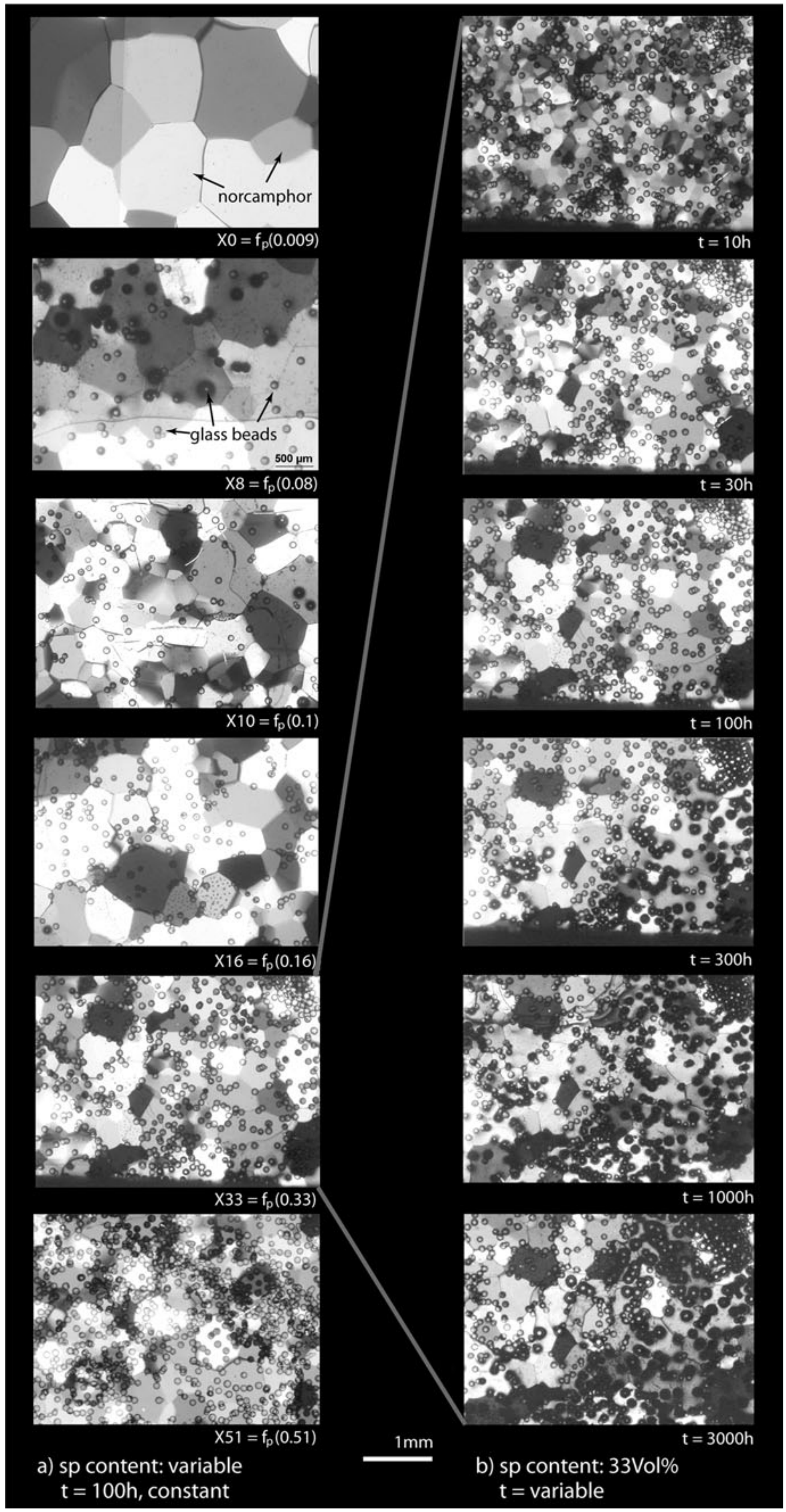

Fig. 1 Microstructural evolution in the experiments. *Left column*: increasing volume fraction of micro glass beads (small spheres) ranging from nominally 'pure' (without glass beads but f_p of 0.009, top micrograph) over 0.08, 0.10, 0.16, to 0.33 in the lowermost micrograph. Norcamphor grain size (matrix) decreases from top to down with increasing f_p. All micrographs taken at $t = 100$ h after experiment set-up. *Right column*: Micrograph sequence of experiment X33 with an f_p of 0.33 at time intervals of 10, 30, 100, 300, 1,000 and 3,000 h after experiment set-up. Norcamphor grain size increases until grain boundaries become immobile (>300 h)

Table 1 Summary of information about all experiments discussed in the text

Experiment no.	Run-time (h)	Thickness (μm)	D at 100 h (μm)	D_{max} (μm)	f_p	d_p (μm)	Z (μm)	n	n-fit	k	k-fit
'Pure'1	2,745	400	919	1,271	0.009	53	5,889	4.5504	5.76	2.87E + 11	2.86297E + 11
'Pure'2	155	280	887 (90 h)	980	0.017	30	1,765	4.5504	5.76	2.87E + 11	2.86297E + 11
X08	1,000	140	582	781	0.08	86	1,025	4.1715	4.09	3.37E + 09	8.088E + 09
X10	600	140	571	742	0.1	101	967	3.2354	4.02	8.20E + 06	4.77E + 09
X16	4,450	140	531	718	0.16	107	645	3.7017	3.57	1.22E + 08	1.21E + 08
X33	2,015	140	397	469	0.33	120	357	2.896	3.00	5.27E + 05	5.58E + 05
X51	1,000	140	385	405	0.51	165	323	3.3958	2.91	7.40E + 06	2.26E + 05

digital image sequences under different polarization conditions (for more details see: Fueten 1997; Goodchild and Fueten 1998; Fueten et al. 2002). All experiments were performed under static conditions and a constant temperature of 50°C, which corresponds to a homologous temperature (T_h) of 0.88. Due to the small vertical load applied after mounting the sample into the Urai-Means rig, slight flattening of the sample occurred during the first 3 hours. This was seen by the minimal movements of the glass beads, which act as passive markers in the norcamphor matrix during this stage. At this time, air that was trapped during cold pressing became interconnected and was pushed out towards the sample rims, leading to a nearly complete elimination of porosity. The termination of flattening is indicated by the immobility of the glass beads, which occurred after 1 h of experiment run-time for all experiments, defining the onset of true static conditions and the starting time t_0 with starting grain size D_0. After 300 h, the sample was removed and placed in an oven for up to 4,450 h. The experiments were terminated when the adhesive embrittled due to continuous heating reducing the sealing effect for preservation of the gas pressure of norcamphor. In the first 40–50 h, while norcamphor grain sizes were still small, images were acquired at high magnification and at time intervals of 30 min. Due to progressive grain growth, the magnifications were then reduced to obtain a statistically sufficient number of grown norcamphor grains. During this second interval (50–300 h) images were acquired every hour. Once the sample was placed in the oven, time-lapse intervals between individual images were increased to 250 h. In this way, a continuous tracing of the growth history of individual grains was possible, especially during the fast-evolving first 300 h of the experiments, when significant microstructural changes occur relatively rapidly. Animations showing the microstructural evolution of the experiments are available from the authors upon request.

Based on the acquired images, digital image processing and analysis routines were carried out to quantify the grain growth of norcamphor as a function of the second-phase content and time. For this purpose, grain boundaries of norcamphor and glass beads were traced manually, using Adobe Photoshop®. Note that only the most homogeneous areas where glass beads were distributed as regularly as possible were selected for microstructural analysis and large analysis areas were chosen to average out potential local heterogeneities in distribution. The grain boundary images were analysed with Image SXM (Barrett, see www.liv.ac.uk/~sdb/ImageSXM) to quantify the grain areas of second phases and norcamphor. From the grain areas, the volume fraction (f_p) and number-weighted grain size (d_p) of the second-phase particles, as well as area-weighted grain size (D) of the norcamphor matrix grains were calculated. The calculation and advantage of using area-weighted mean grains sizes are discussed in Ebert et al. (2007). Note that due to some heterogeneities in the spatial distribution of the glass beads within the norcamphor matrix, i.e. clustering for high f_p (Olgaard and Evans 1986; Weygand et al. 2000), the x- and y-coordinates of the second phases were additionally measured with the image analysis procedure. Based on these data, the nearest neighbour distances between neighbouring second phases were calculated. Additionally, time-lapse sequences with a time interval of 10 h were created in order to study grain-scale processes in the vicinity of second phases. One grain of experiment X16 was selected and observed in detail during the time interval 30–230 h. This time period was chosen due to 2-D grain growth. To detect the time-dependent displacements of individual grain boundaries, vectors normal to the grain boundaries were constructed. For this purpose, we chose the 2-D period and used only the grain boundaries situated along the upper glass plate to calculate the corresponding displacement vectors of grain boundaries parallel to the glass plates, thus dealing with it similarly to an ordinary thin section of a rock. This treatment was applied for the sake of simplicity, well knowing that the displacement vectors are three-dimensional features. Since in this study we are interested only in relative displacements per time increment, the aforementioned simplification is justified. The length of a vector is defined by the distance between two grain boundary positions given at two successive time intervals of Figs. 5 and 6.

The resulting datasets allowed investigations in two different directions: (1) The analysis of grain–neighbour relationships requiring high spatial and temporal resolution, and (2) the microstructural evolution of the entire aggregates requiring long-term observations and sufficient grain statistics. The latter dataset was used to generate a modified grain growth law for polymineralic systems.

Results

Evolution of the bulk aggregates

Figure 1 shows the microstructural development of six different experiments (left column), starting with a nominally 'pure' norcamphor sample without glass beads (experiment X0 with f_p of 0.009; top micrograph) followed by experiments with increasing glass bead volume fractions (f_p) of 0.08 (X8), 0.10 (X10), 0.16 (X16), 0.33 (X33) and 0.51 (X51, all in Table 1). Each micrograph was taken after a time interval of 100 h. Compared to the initial microstructures, the norcamphor grain size increases with decreasing glass bead content and shows the largest grains in the pure experiment (top left). The right column of Fig. 1 shows the time-dependent microstructural evolution of Experiment X33 (f_p of 0.33) at time intervals of 10, 30, 100, 300, 1,000 and 3,000 h of experiment run-time. A grain size increase can be observed in the first 300 h. After 300 h of experiment run-time the grain boundaries become immobile and the grain size stabilized.

This second set of micrographs (>300 h), as well as the temporal evolution in grain size for all experiments (Fig. 2), indicate that grain growth is not continuous on the grain-scale for the whole run-time of each experiment. As shown in Andrade and Aboav (1966), and in Fig. 9 in Covey-Crump and Rutter (1989), our experiments reveal different stages of grain growth. Due to the small initial grain size (<50 μm) and sample thicknesses generally around 140 μm, three-dimensional overlap prevents an accurate grain size analysis during the first increments of the experiments. Hence, stage I of "rapid grain growth" of Andrade and Aboav (1966) cannot be analyzed and is therefore missing in our datasets. But with proceeding time, 3-D grain growth becomes delimited by the glass plates between which the samples are confined, changing into a 2-D grain growth with growth vectors parallel to the plane of view. As a consequence, only three out of the original four stages of Andrade and Aboav (1966) can be discriminated in our experiments: during the first part of the 2-D growth, grain size increases with proceeding time (stage II), followed by a transitional period of reduced grain growth (stage III), ending with a stabilized grain size that does not change anymore with proceeding time (stage IV). Characteristically, pure norcamphor aggregates (diamond symbols) show larger grain sizes than the experiments containing glass beads (circles, see Fig. 2). Additionally, the onset of stages III and IV are different for each experiment, occurring earlier with increasing f_p and, therefore, resulting in a smaller matrix grain size. Consequently, stabilized grain size (stage IV) is reached earlier and at smaller grain sizes for high f_p of glass beads than for low f_p (Fig. 2).

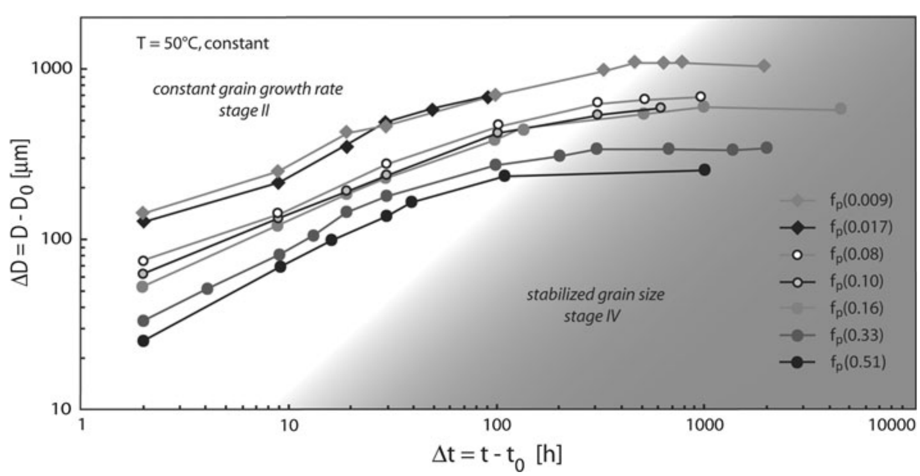

Fig. 2 Mean matrix grain size evolution for all experiments. Stage II characterized by a constant grain growth rate and stage IV characterized by a stabilized grain size (cf. text). For pure norcamphor experiments (*diamonds*) mean grain sizes are larger than for two-phase experiments (*circles*), and grain sizes are smaller the higher f_p. Analogous to a higher f_p, the onset of the field of a stabilized grain size is earlier. Note that the experiment with an f_p of 0.10 (*grey circles* with *black* rim) has only slightly larger grain sizes than the one with an f_p of 0.16 (*grey circles*)

These results are also confirmed by the evolution of grain-size distributions (Fig. 3): both the mean grain size and the width of the grain size distribution decrease with increasing f_p (first column) after 3 h. While the mean values for all two-phase systems range between 176.3 and 237.1 µm, the pure aggregate shows a considerable larger mean grain size of 390.9 µm. The mean grain size of the experiment with the highest f_p of 0.51 is not smallest, as was intuitively expected, but yields values between the ones of the experiments with $f_p = 0.16$ and $f_p = 0.33$. After 1,000 h of experiment run-time (second column), all experiments have passed into microstructures of stage IV with a stabilized grain size that show symmetric Gaussian-type grain size distributions. Here, the mean value of 1271.6 µm for the pure aggregate is more than three times larger than that for the experiment with the highest second-phase volume fraction (f_p: 0.51, D: 405.2 µm). Experiment X10 shows a smaller mean grain size of 652.2 µm than experiment X16.

From a morphological point of view, grain shapes evolve differently as a function of time and second-phase volume fraction: in case of nominally pure samples, typical foam textures develop, as observed in other experiments as well as numerical modelling approaches (e.g. Covey-Crump 1997; Jessell et al. 2001, 2003). Associated with the formation of foam structures is the evolution of isometric grains, as well as straight to slightly curved grain boundaries typical of static grain growth. In contrast, second-phase rich samples are characterized by grooved matrix grain boundaries and non-isometric and irregularly shaped grains that even persist within the field of stabilized grain size (stage IV, see Fig. 1 at $t = 3{,}000$ h).

The heterogeneity in distribution of glass beads is visible in the microstructures documented in Fig. 1 (left column, compare e.g. upper right corner with adjacent parts of image X33) and the histograms of columns 3 and 4 in Fig. 3, where inhomogeneous dispersion and clustering of second-phase particles can be observed. Spatial heterogeneity in dispersion increases with increasing volume fraction of glass beads. Hence, subsequent changes in inter-particle distances between second-phase particles as a function of second-phase volume fraction are obtained (Fig. 3, column 4). With increasing volume fraction, interparticle distances decrease and are reduced to the minimum mean value of all experiments of 211.8 µm for an f_p of 0.33. In addition, clustering of the second-phase particles occurs with increasing f_p (Fig. 3, column 3). The appearance of clusters is relatively rare up to $f_p = 0.16$. Cluster sizes of around 120–140 µm are related to accumulations of two to three glass beads, and only up to 10% of the counted second phases is affected by clustering for $f_p = 0.08$ and 0.10. From $f_p > 0.16$ on, the amount and the size of the clusters increase dramatically from 23 to 63%, and to 80% of counted second-phase particles, respectively, for $f_p = 0.16$, $f_p = 0.33$ and $f_p = 0.51$. In these agglomerates up to ten individual glass beads can be involved. In context of the microstructural response, clustered glass beads were treated as individual, but larger second-phase particles (Fig. 4). In this figure, the aforementioned pronounced clustering in experiment X51 becomes obvious, resulting in an extraordinary large particle/cluster size of 164.9 µm, which is larger than the extrapolated trend of Fig. 4. This fact, as well as an $f_p > 0.5$, requires an exclusion of this experiment X51 from any further calculations. In the case of the two pure samples, f_p of 0.009 and 0.017 were estimated. Note that these f_p result from few dust particles which are present in the nominally pure aggregates. The spacing of the dust particles is at any time much larger than the matrix grain size. Thus, the effect of the bulk particles on the average aggregate grain size is limited and will not be considered further.

Fig. 3 Histograms of matrix grain size evolution, second-phase grain ▶ sizes and second-phase nearest neighbour correlation of experiments from pure (*top*) to f_p of 0.08, 0.10, 0.16, 0.33 and 0.51 (bottom). *Column 1* histograms of matrix grain sizes after 3 h. *Column 2* histograms of matrix grain sizes after 1000 h, i.e. for stabilized grain sizes (stage IV). *Column 3* histograms of second-phase grain sizes. Grain size classes of 70–100 µm represent individual, unclustered glass beads (*shaded area*, mean glass bead diameter: *dashed line*), whereas grain sizes of around 120, 140, 160 µm and more refer to clusters of 2, 3, 4 and up to several tens of glass beads, respectively. *Column 4* histograms of nearest neighbour distances for second phases. Distances in micrometer were calculated from centre to centre of the second phases

Grain-scale observations

Based on the series of high-resolution images described earlier, grain A (Fig. 5) of experiment X16 was selected and observed in detail. Figure 5 shows a correlation between the view from above (top row) and a three-dimensional perspective (bottom row). It can be clearly seen that at time 30 h the 2-D grain growth state for grain A is reached and kept until the end of this experiment observations. Compared to the continuous grain size increase of the bulk aggregate, grain A shows a step-like growth behaviour manifested by stages of accelerated and reduced growth velocity (Fig. 6). This difference is based on variations in grain boundary displacements of the individual grain segments, which depend on the occurrence and effect of second-phase particles on the moving grain boundary segments. For example, the displacement of vector ‘a’ is zero over the entire time period, indicating a complete pinning of this grain boundary segment by glass beads 5 and 6 (Fig. 6). In contrast, vector h_1 reflects a

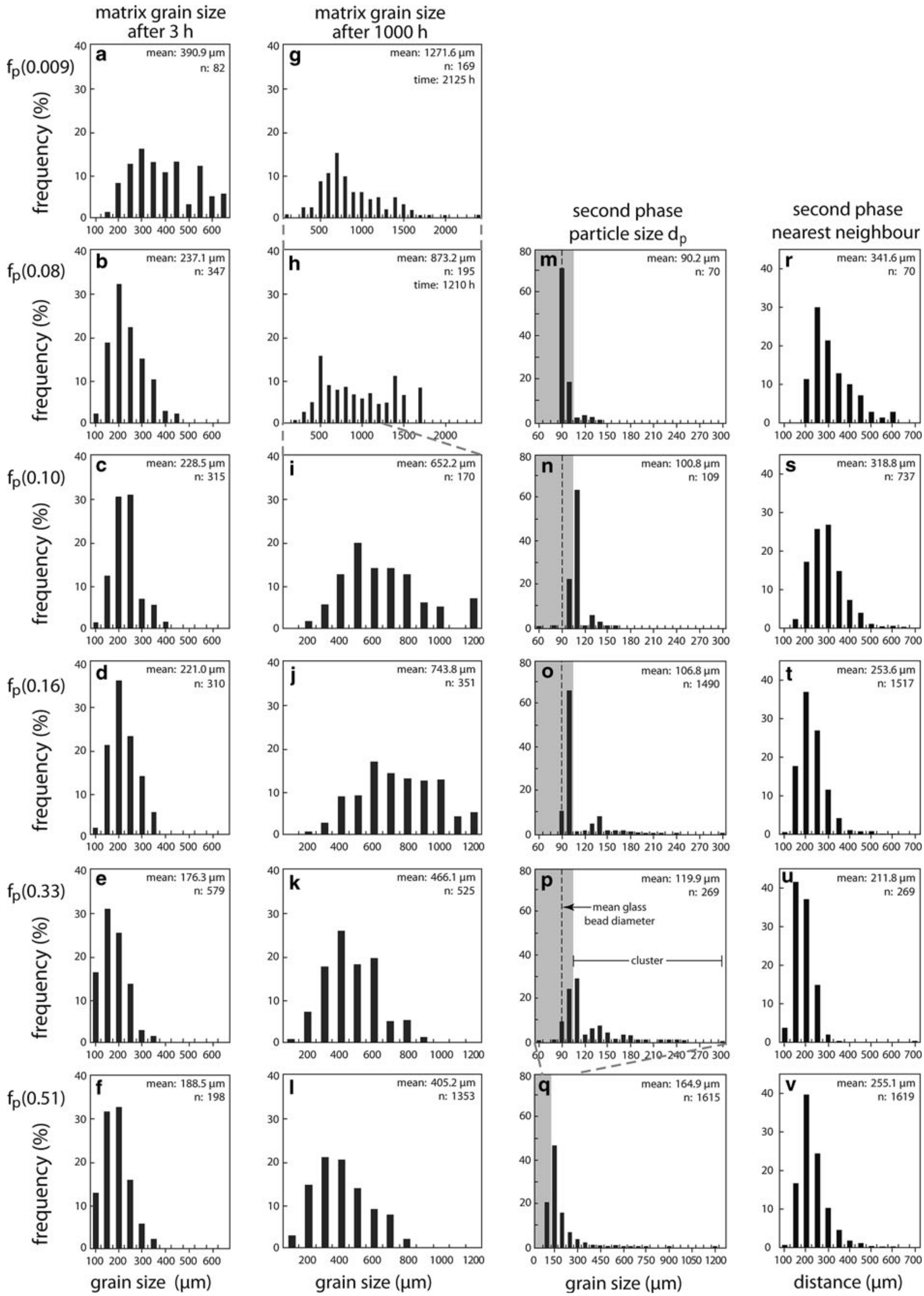
matrix grain size after 3 h
matrix grain size after 1000 h
second phase particle size d_p
second phase nearest neighbour
f_p(0.009)
f_p(0.08)
f_p(0.10)
f_p(0.16)
f_p(0.33)
f_p(0.51)
frequency (%)
a mean: 390.9 µm n: 82
b mean: 237.1 µm n: 347
c mean: 228.5 µm n: 315
d mean: 221.0 µm n: 310
e mean: 176.3 µm n: 579
f mean: 188.5 µm n: 198
g mean: 1271.6 µm n: 169 time: 2125 h
h mean: 873.2 µm n: 195 time: 1210 h
i mean: 652.2 µm n: 170
j mean: 743.8 µm n: 351
k mean: 466.1 µm n: 525
l mean: 405.2 µm n: 1353
m mean: 90.2 µm n: 70
n mean: 100.8 µm n: 109
o mean: 106.8 µm n: 1490
p mean: 119.9 µm n: 269
mean glass bead diameter
cluster
q mean: 164.9 µm n: 1615
r mean: 341.6 µm n: 70
s mean: 318.8 µm n: 737
t mean: 253.6 µm n: 1517
u mean: 211.8 µm n: 269
v mean: 255.1 µm n: 1619
grain size (µm)
grain size (µm)
grain size (µm)
distance (µm)

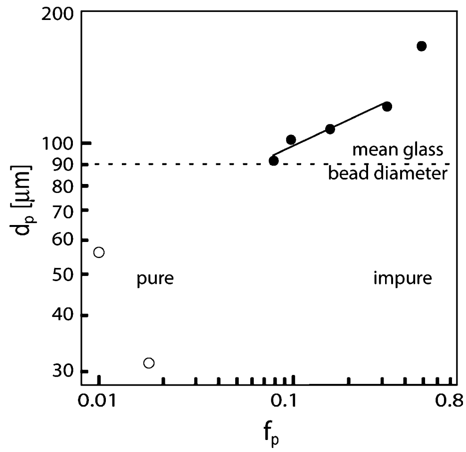

Fig. 4 Dependence of average second-phase particle/cluster size on volume fraction. The higher the second-phase volume fractions (f_p) the higher the probability of the occurrence of clusters of second phases, which results in larger second-phase particle sizes (d_p). Average size of single, unclustered glass bead is indicated by the *horizontal dotted line*. Experiments with clustered glass beads and consequently higher second-phase particle size d_p lie above the *dotted line*, while the pure norcamphor experiments without glass beads but other second-phase particle types have a smaller d_p. The value for experiment X10 is slightly above the trend, as already visible in Fig. 3g. Pure experiments and X51 are not included in the calculations of the regression line

pronounced grain boundary velocity during the first 70 h of the experiment followed afterwards even by a retreat of the boundary. This retreat results from the growth of a neighbour grain inducing a local shrinkage of grain A. A third type of interaction between a norcamphor grain boundary with a second-phase particle is demonstrated by the growth vectors f_1 and f_2, which reflect a grain boundary passing glass bead number 2. Here, the grain boundary velocity is dramatically enhanced at about 130 h owing to the detachment of the grain boundary from the glass bead (Fig. 6). This accelerated growth continuous until the freed grain boundary is affected again by glass beads of the second-phase cluster number 8. Pinning at glass bead 2 nicely demonstrates that grain boundary movements, at least in the early stages of grain growth, also involve a 3-D component. The grain boundary segments of growth vectors f_1 and f_2 dip westwards, while being pinned at glass bead number 2 (Fig. 5a bottom). After the detachment, the entire grain boundary turns into a subvertical orientation when becoming pinned again by glass bead cluster number 8 (Fig. 5b, bottom). Besides glass beads, also triple junctions reduce the migration velocities of grain boundaries or can even induce their stabilization (Fig. 6). The growth history of grain A, for example, is therefore defined by the sum of all these local influences on the grain boundaries. If one of these local processes temporarily dominates, this might induce a substantial change in area, which will be manifested by a change in the growth behaviour of the entire grain.

Compared to grain growth of the bulk aggregate (white triangles in Fig. 6d), grain growth of grain A (white

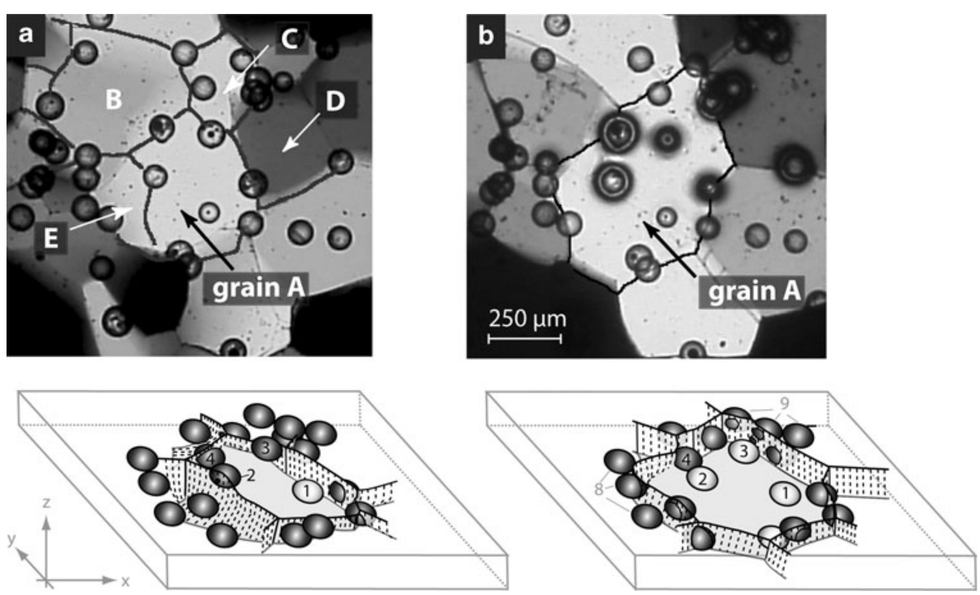

Fig. 5 Micrographs (*top row*) and 3D block diagrams (*bottom row*) of the evolution of grain A of experiment X16. *Bright spheres* in the block diagrams represent glass beads included in the interior of grain A. **a** Grain A after 40 h of grain growth. Note the deflection of the western grain boundary of grain A due to pinning by glass bead number 2. Here, as well as at glass bead number 4, the norcamphor grain boundaries are inclined. **b** With progressing grain growth grains B, C, D and E become consumed by grain A, but the grain boundaries of grain A become increasingly affected by glass beads. At this stage (210 h), most of the norcamphor grain boundaries are subvertically oriented and are either pinned by individual glass beads, by glass-bead clusters (e.g., clusters 8 or 9) or by triple junctions

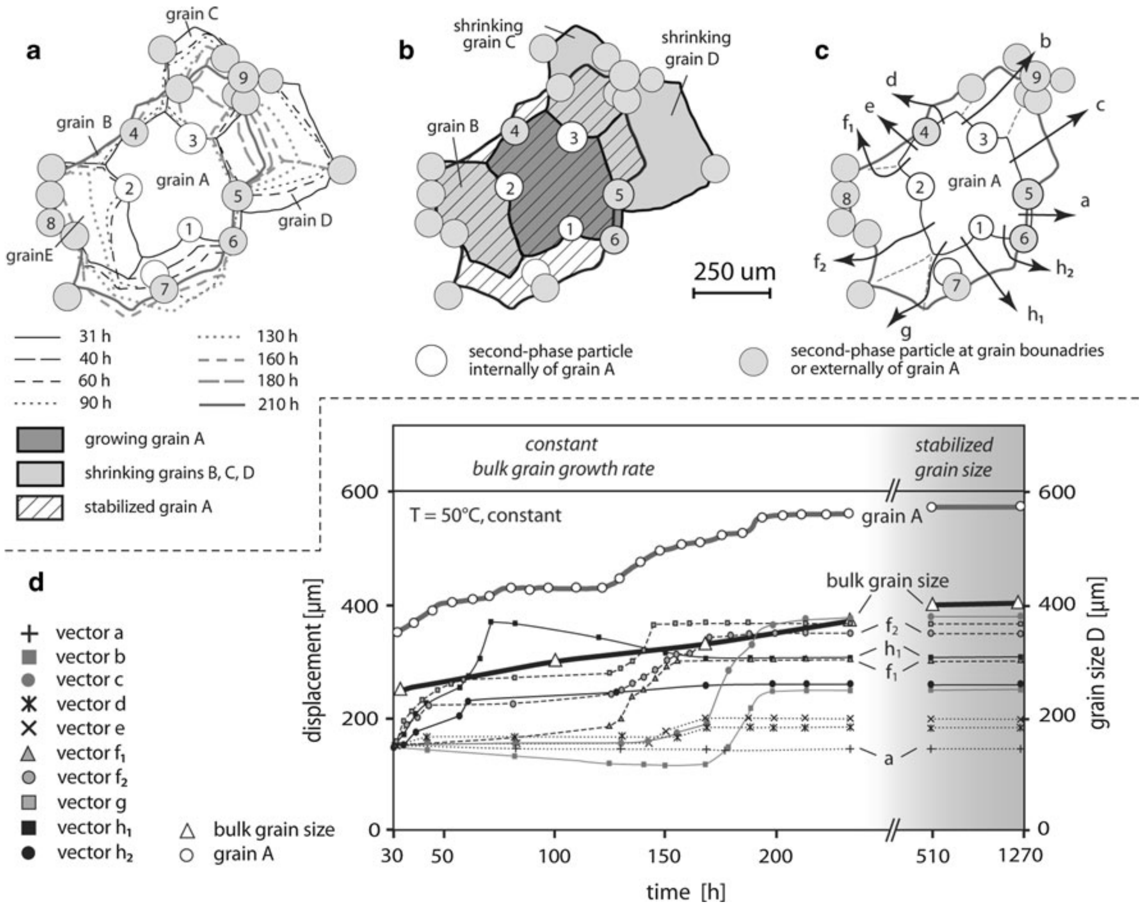

Fig. 6 Drawings of the growth evolution of grain A using grain boundary outlines along the upper glass plate. **a** Outlines of different growth stages of grain A indicated by continuous and *dashed line* signatures including the three surrounding shrinking grains (**c**, **d** and **e**). Second phases entirely included in grain A are *white*, those at the grain boundaries or external of grain A are *grey*. **b** Grain boundary map of starting (*dark grey*) and final (*striped*) stages of grain A including the three shrinking grains (*light grey*) in its neighbourhood. **c** Labels of all second-phase particles, clusters and individual displacement trajectories of grain boundaries. The *dotted lines* show the relation of the grain boundaries during earlier growth stages. **d** Grain growth of bulk aggregate and grain A as well as individual displacement trajectories of grain boundaries as a function of increasing experiment run-time (**a**). After 30 h of experiment run-time, the size of grain A (*white circles*) is already larger compared to the average bulk grain size (*white triangles*). Growth vectors are calculated from an artificial centre point of grain A at 30 h and show substantial variations indicating stages of reduced and accelerated grain boundary velocities. The latter occurs just after detachment of a previously pinned grain boundary (e.g., see growth vector f_1 after 130 h)

circles) is more pronounced. This difference between grain A and the bulk aggregate is the result of the averaging over the growing and shrinking grains in the latter. In this way, also local 'events' of accelerated growth of individual grains diminish as can be inferred from the smooth and steadily increasing growth curve of the bulk aggregate compared to the more irregular grain growth history of grain A (Fig. 6d).

Discussion

The following discussion is divided into three parts: the first part deals with potential artefacts associated with the experimental treatment. In the second part, we discuss the microstructural evolution and related processes during grain growth, while in the third part a parameterization of the observed processes will be given in the form of a mathematical model for matrix grain growth in second-phase affected aggregates.

Potential artefacts of the rock analogue experiments

It applies for any experimental investigation and for any see-through rock analogue experiments that potential artefacts related to the experimental procedure have to be considered. With this respect, we will discuss in the following two major aspects: (1) effect of compaction-induced internally stored energy on grain growth and (2) the effect of 2-D versus 3-D grain growth.

(1) Owing to cold pressing and subsequent compaction during the initial experimental stages (see above), grain internal deformation by the evolution of dislocation substructures has to be taken into account. This fact can be critical, because intragranular differences in defect structures can act as additional driving force for grain boundary migration (e.g. Urai et al. 1986). In our experiments, we believe that the compaction-induced strain energy can be neglected for the following reasons: (a) A major amount of compaction is related to the reduction of porosity. In this way, the sliding of grain boundaries along each other will be the predominant processes. Potential accommodation mechanisms of grain boundary sliding could be plastic deformation or dissolution-precipitation processes. If important, both accommodation mechanisms would yield in shape preferred orientations, which is not the case in our experiments. Furthermore, grain internal plastic deformation must be rather limited as indicated by the lack of undulose extinction and subgrains (Fig. 1). (b) Before capturing the first image, a grain size increase of a factor > 3 occurred. As stated by Bons et al. (2000) for static grain growth in OCP, initial recrystallization and growth is driven first by stored energy but diminishes with progressive sweeping of grain boundaries. Similar to their study, we started with grain-size analysis in our experiments not before foam textures with equidimensional grains developed, which we interpret to result from surface energy as dominant driving force for grain growth. Nonetheless, we cannot fully exclude that a small portion of stored deformation energy survived in the cores of the grains (Jessell et al. 2003). The influence on bulk grain growth, however, will continuously decrease with increasing grain size and become of subordinate importance.

(2) Generally, the sample thicknesses in the experiments are 140 µm (except for the pure norcamphor experiment with a thickness of 320 µm, Table 1). The norcamphor grain size increases from a few micrometers after cold pressing up to 1 mm in the case of stabilized grain sizes in the pure norcamphor experiments (Fig. 2). Based on these dimensions, a real 3-D growth of norcamphor grains is possible during early stages of grain size evolution, while with increasing grain size the 3-D grain shapes are limited by the glass plates. At this stage, the norcamphor grain boundaries typically are perpendicularly oriented to the glass plates and any grain boundary migration occurs along vectors parallel to the glass plates only (Figs. 5b and 6c). The question arises as to what are the effects of the changes from 3-D to 2-D growth behaviour. First of all, detection of grain boundaries during early growth stages is difficult because of potential vertical overlap of different grains or grain boundaries not perpendicularly oriented with respect to the glass plates. These problems can be reduced by (1) starting grain boundary tracing only after certain stages of grain growth (see above) and (2) by using area-weighted grain-size estimates (e.g. Herwegh and Berger 2004; Ebert et al. 2007). In the latter case, large grains are volumetrically more important compared to smaller grains, the latter being more critical in terms of 3-D growth and related detection artefacts. (3) Moreover, considering a statistically sufficient number of grains for the grain-size analyses will result in an averaging out of potential 3-D artefacts. In light of a change of 3-D to 2-D grain growth behaviour, we see a constantly increasing grain size (Fig. 2), without any change in slope as could be expected in the case of a kinetic effect on 3-D and 2-D growth. Moreover, the thickness of the experiment seems to have no deviant influence. For the pure experiment with the thicker sample size, 3-D grain growth is consequently longer possible and therefore, grain size is expected to be smaller in 2-D view. But due to the unhindered grain growth, this 3-D period is not longer than for samples containing glass beads. Additionally, all glass-bead bearing experiments show a correlation between the second-phase content and the matrix grain size (Fig. 2), while the thickness of all these samples is identical (140 µm, Table 1). We therefore conclude that the effect of second phases on the matrix grain size is the major effect on grain growth. In addition, also the pinning of matrix grain boundaries by triple junctions or impurities contributed to the overall immobilization of grain boundaries as indicated by grain size stabilization in the pure samples (see also below). All these points mean that any potentially existing difference between 3-D and 2-D grain growth must be rather weak in the case of our norcamphor experiments. The same argumentation also suggests that neither a detectable enhancement nor a reduction in grain boundary migration velocity by lubrication or pinning, respectively, takes place at the norcamphor-glass interface. As a consequence, we believe that during grain growth artefacts related to the 2-D versus 3-D problem as well as an effect of the glass plates on the velocity of grain boundary migration are of limited importance only. To conclude, we will use in the following the entire time period of constant grain growth to characterize the effect of second phases on grain growth of the norcamphor matrix (Fig. 2).

Microstructural evolution and related processes

Basics of grain growth

For monomineralic rocks and materials, constant normal grain growth is described by equation 1 (Simpson et al. 1971; Poirier and Guillopé 1979; Olgaard and Evans 1986):

$$D^n - D_0^n = k \cdot (t - t_o) \quad (1)$$

The dimensionless growth factor n is an exponent to the grain size D [μm] and the starting grain size D_0 [μm], while k is a growth constant depending on n and $(t - t_0)$ is the time interval referring to D. In theory, the growth exponent n is unique for the same materials at identical conditions (P and T). For differing conditions, but the same materials, n can be attributed (in case of pure systems) to different growth-rate limiting processes like surface diffusion and lattice diffusion (Evans et al. 2001 and references therein). In practice, however, an unambiguous attribution to a specific growth process is often difficult, due to the fact that different processes show similar n values, which replace or even superimpose each other (e.g. Brook 1976). Incorporating a temperature dependence into Eq. 1 allows the extrapolation of a grain growth law to natural conditions (e.g. Covey-Crump and Rutter 1989; Herwegh and Berger 2003).

In nature, rocks are rarely monomineralic, and the grain coarsening behaviour of polymineralic rocks is largely unknown. In rocks with a predominant matrix phase ($f_p > 0.5$) the second phases impose dragging forces on the migrating grain boundaries, and thus counteract surface energy resulting in a retardation of grain growth. Such pinning of grain boundaries is mainly a function of the volume fraction f_p, particle size d_p and dispersion of the second phases (see Fig. 3 in Herwegh and Berger 2004). Zener (in Smith 1948) was among the first who related the maximum matrix grain size D, i.e. the related curvature, with the effect of second phases (with c as a constant):

$$D = c \cdot \frac{d_p}{f_p} \quad (2)$$

Based on a large number of experimental studies in material sciences, a broad variety of mathematical expressions exist to express the matrix grain size (see Table 1 in Olgaard and Evans 1986; see Table 2 in Manohar et al. 1998; Hillert 1965; Srolovitz et al. 1984; Nes et al. 1985). Generally, solid and liquid/gaseous second phases have to be discriminated as they behave in rigid and deformable manner during pinning, respectively (Evans et al. 2001; Petrishcheva and Renner 2005).

It will be shown that the influence of second phases cannot yet be described in a proper way by Eq. 1. As will be discussed in more detail below, the growth exponent n for example, varies with the second phase content. In order to successfully extrapolate a grain growth law to nature, the effect of second-phase particles on grain growth of a matrix phase has to be integrated into Eq. 1. In the following, we focus on different manners of pinning of the solid type in case of our impure samples.

Single particle pinning (SPP)

In accordance with the previous studies on grain growth, all our experiments show increasing grain sizes with proceeding time on the aggregate-scale during stage II and are stabilized in stage IV (Fig. 2). The dependence of grain size evolution on amount and dispersion of second phases raises the following questions:

– How do glass beads affect grain growth on the grain-scale?
– What is the effect of amount and dispersion of second phases on bulk grain growth?
– What controls the finally stabilized matrix grain size?
– Why do timing and transition of stage III depend on the amount of second phases?

In literature, the effects of second phases on migrating grain boundaries are well described (e.g. Smith 1948; Nes et al. 1985; Evans et al. 2001). Under static conditions in monomineralic pure materials, the driving force for grain growth is based on the reduction of surface energy, which is manifested by the curvature of the grain boundary (Evans et al. 2001). In this sense, the larger the grain sizes the lower the grain boundary curvature and the lower the surface energy. Generally, the velocity V of the migrating grain boundary during grain growth is linearly expressed as a function of the product of total driving force F and the boundary mobility M (Brook 1976; Poirier and Guillopé 1979; Dresen et al. 1996; Rios et al. 2002):

$$V = M \cdot F \quad (3)$$

The intrinsic grain boundary mobility of a material depends on a variety of parameters like temperature, diffusivity, grain boundary width, Boltzmann factor and the unit cell volume (e.g. see Eq. 10 in Evans et al. 2001). Furthermore, chemical impurities and second phases, as commonly found in natural rocks, can influence the grain boundary velocity by counteracting the driving force F (Olgaard and Evans 1988; Freund et al. 2001; Rios et al. 2002). Particularly, second phases impose a drag on the grain boundary, described by the pinning force F_{pin}, allowing a modification of Eq. 3 (Brook 1976; Poirier and Guillopé 1979: therein Eq. 3):

$$V = M \cdot \left(F - F_{pin}\right) \quad (4)$$

As long as $F_{pin} < F$, the grain boundary is still able to migrate, but at reduced velocity, because the total driving force is reduced by F_{pin}. Absolute pinning of the grain boundary is obtained, when $F_{pin} \geq F$ at the contact point between matrix phase and second-phase particle (Manohar et al. 1998). In our experiments, such pinning behaviour occurs throughout the whole aggregates (Fig. 1) and is reflected, for example, in case of grain A by glass beads 4 and 6 (cf. Figs. 5, 6). Based on the experiments (grain A and glass bead 2), we generalized the changes in geometry and velocity as a migrating norcamphor grain boundary passes a spherical second-phase particle (Fig. 1 of electronic supplementary material).

In this schematic 2-D illustration, the grain boundary is divided into three sections *a*, *b* and *c* with corresponding section velocities V_a, V_b and V_c. It approaches a glass bead (time step 1), is mitigated in the following by the glass bead (time steps 1–7) until the grain boundary is detached (time step 7) and migration can continue. Before time step 1, the grain boundary migrates with a specific velocity V, but when approaching the glass bead (time step 1) the grain boundary experiences a weak attraction as a consequence of the mutual attractive polar behaviour of both phases (pers. communication Roman Leist). As a result, the velocity V_a and the curvature of grain boundary section *a* have a higher value than the corresponding values for sections *b* and *c*. After having approached the glass bead, V_a is still higher than V_b and V_c due to this attraction, resulting in a slightly negative curvature of the grain boundary geometry at *a* and *b* at time step 2. Despite the negative curvature and therefore a reduced driving force F, the grain boundary is still moving onward. The authors suggest here a combination of two effects: (1) the strongest influence is given by surrounding grains. If the driving forces of adjacent grains are still smaller or disadvantageous compared to the growing grain with a negative curved grain boundary, then the latter grain will continue to grow. (2) During time steps 1 and 2, the polar attraction has a stronger influence than the negative curvature and equalizes the reduction of the driving force.

As soon as the grain boundary comes into contact with the glass bead, V_a is reduced at the contact point to the second phase by the latter's restricting pinning influence (F_{pin}) on the grain boundary mobility and its minimizing effect on the driving force F (time steps 3 and 4). With increasing distance from the second phase (sections *b* and *c*), however, the effect of F_{pin} ceases and the grain boundary velocity is less decelerated. If the total driving force F is always larger than the pinning force F_{pin} (Eq. 4), the grain boundary is not fully pinned at the contact to the glass bead and V never drops to 0, but is slow (cf. vectors d and e in Fig. 6d). At times 2–6 (Fig. 1 of electronic supplementary material), the wetting angle of the grain boundary to the glass bead remains at 90° (Evans et al. 2001) and, therefore, the grain boundary at section *a* slowly moves along the rim of the second-phase particle. At time 5, curvature of section *a* is at a maximum, but it has minimum velocity one time sequence later. At time 6, no further migration of the grain boundary along the rim of the second-phase particle is possible any more. At this time, F_{pin} reaches its maximum in section *a*, and simultaneously, the curvature at sections *b* and *c* is largest loading the grain boundary fully, and therefore, forcing a detachment of the grain boundary from the second-phase particle and a immediate decrease of F_{pin} to 0. As a consequence of Eqs. 3 and 4, this will result in a very fast migration of the grain boundary mainly at section *a*, which in fact can be observed in our experiments in the case of the detachment of the grain boundary at glass bead 2 (vector f_1, f_2 and g; 125–150 h, Fig. 6d) or the detachment at glass bead 3 (vectors b and c at time interval 170–200 h in Fig. 6d). Due to progressive migration (time step 5), the curvature reduces again in the following and so do the driving force and velocity of the grain boundary (Fig. 1 of electronic supplementary material).

After having passed a second-phase particle in the aforementioned manner, the process of pinning, overgrowth and detaching is repeated for the grain boundary when reaching the next second-phase particle. Therefore, the migration of a specific grain boundary can be step-wise, which is characterized by a slowed down or even stopped and accelerated velocity, during and after pinning, respectively (see vectors g and f_2 in Fig. 6). For a single grain, pinning and normal grain boundary migration may occur simultaneously at different grain boundaries. In light of grain growth, i.e. the net migration of all grain boundaries, a step-wise change in the grain's size will occur as visible in Fig. 6 during the growth history of grain A.

Multiple particle pinning (MPP)

With increasing second-phase volume fraction the particles are closer to each other and, therefore, the probability for a specific grain boundary to influence several particles aligned to each other is increased. Thus, the pinning effect on the grain boundary is a sum of the forces exerted by each second-phase particle and so depends on the position of each particle relative to the boundary (Manohar et al. 1998; Miodownik 2005). In comparison to the single-particle case described above, a local grain boundary curvature can hardly evolve in this multiple-particle situation, because the particles are too closely situated to each other to overcome the influence of the second-phase particles (cf. glass beads 5 and 6 in Fig. 6a: corresponding growth vector 'a' in Fig. 6d). As a result of this multi-particle influence, the entire grain boundary can become completely immobilized for the whole experiment duration, as we observed for stage IV in all two-phase experiments.

Clustered particle pinning (CPP)

As mentioned earlier, clustering of the second-phase particles (see Figs. 1, 3, 4) becomes prominent with increasing f_p, which again modifies the general pinning intensity (Fig. 7). Due to clustering, several individual second-phase particles touch each other, resulting in a larger 'particle/cluster size' (Fig. 3, column 3, and Fig. 4) and 'particle/cluster surface'. Clustering, i.e. larger second-phase grain sizes result in smaller matrix grain sizes (Kad and Hazzledine 1997) because they impose higher pinning forces as the pinning force F_{pin} is directly dependent on the radii of the second-phase particles (Manohar et al. 1998 and references therein; Evans et al. 2001). Consequently, the cluster cannot be overcome by a moving grain boundary anymore. Clustering in our experiments occurs for volume fractions >0.1, but it influences the grain growth behaviour more prominent for $f_p \geq 0.33$ (Fig. 7). This correlates with numerical modelling approaches of Moelans et al. (2006), which predict an influence of clustering for second-phase volume fractions larger than 0.3.

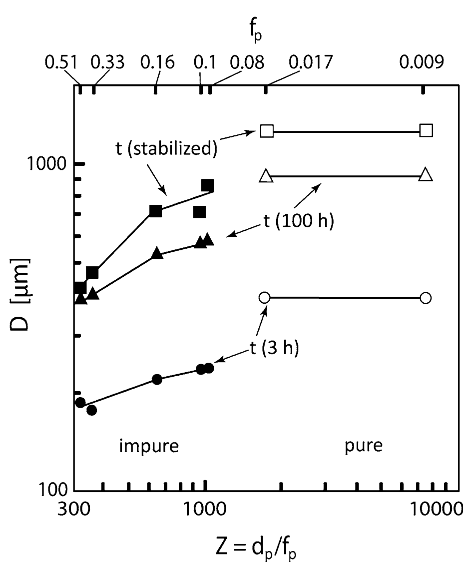

Fig. 7 Relationship between matrix grain size and Zener parameter with proceeding experiment-time. Matrix grain size D increases with increasing Zener parameter Z (and decreasing f_p) and time t. While the two pure experiments (*white symbols*) are not affected by Zener-related pinning at any time, the impure experiments (*black symbols*) show Zener-affected pinning. At time $t = 3$ h (*circles*) slopes between the experiments are similar, suggesting a similar pinning type for all experiment (*black circles*). With proceeding time ($t = 100$ h, *triangles*; $t =$ stabilized stage, *squares*), the slope between f_p 0.51 and 0.16 becomes steeper than the slope between f_p 0.16 and 0.08 with decreasing Z, indicating the increasing influence of MPP and CPP (see text)

Figure 7 summarizes the changes in matrix grain size as a function of Z for different time intervals. For stabilized grain sizes, the slopes become steeper with decreasing Z indicating changes in the pinning regime. Towards earlier stages of grain growth, these changes in slope become less pronounced ending in a nearly constant slope at 3 h for all experiments together, suggesting a similar pinning regime for all experiments. During the early stages, the interparticle distances of the glass beads are larger than the matrix grain size (Fig. 3, compare first and fourth column) allowing only a limited amount of matrix grains to be affected by SPP. With increasing matrix grain size, i.e. with proceeding experiment time, individual grains become severely affected by more second-phase particles or clusters (MPP and CPP). This combination of pinning of grain boundaries by second-phase clusters and multi particles enhances the pinning intensity as described earlier. The increasing probability of grain boundaries to be pinned by clusters, i.e. the larger particle/cluster size at higher f_p, is responsible for the steep decline of slope towards lower Z values indicating almost fully pinned microstructures.

Additional parameters affecting grain boundary migration

So far, in this article, the impeding effect on grain size increase was only ascribed to glass beads as second-phase particles. Data from analysed marbles (Mas and Crowley 1996) and computer simulations (Hazzledine and Oldershaw 1990) suggest that for $f_p < 0.05$ and 0.01, respectively, the pinning influence on matrix grain growth is nearly unrestricted. Our pure experiments, without glass beads as second-phase particles, have a second-phase volume fraction in the range of 0.009 to 0.017 and thus lie below the threshold values of restricted grain growth of Mas and Crowley (1996) and Hazzledine and Oldershaw (1990). It is puzzling, however, that our pure experiments pass into the field of a finally stabilized grain size (Fig. 2), suggesting that there have to be additional microstructural features which can affect grain boundary migration. Besides solid particle pinning (I) which we discussed in sections 'Basics of grain growth', 'Single particle pinning (SPP)', 'Multiple particle pinning (MPP)' and 'Clustered particle pinning (CPP)' in detail, and solid nano-scale second-phase particles (II), matrix grain growth can also be affected by deformable second phases like pores (III) and melt films (IV), by pre-existing chemical impurities (V), crystallographic misorientations between adjacent grains (VI) and grain boundary triple junctions (triple junction pinning, TJP) (VII).

(II) Other studies have shown that the segregation of nano-scale second-phase particles can retard grain boundary velocity (Herwegh and Kunze 2002; Berger and Herwegh 2004; Burhan and Ferry 2006).

(III) Pinning by micron to sub-micron-sized pores at grain boundaries (Karato 1989; Olgaard and Fitz Gerald 1993; Dresen et al. 1996; Covey-Crump 1997; Schenk et al. 2005), can remain through incomplete porosity decay during sample preparation.

(IV) The presence of norcamphor melt could account for pinning in form of melt inclusions as found in case of different solid–fluid-phase systems (Renner et al. 2001; Petrishcheva and Renner 2005). In rock-analogue experiments, Bauer et al. (2000a), Rosenberg and Handy (2000), and Streit and Cox (2002) demonstrated that small amounts of water already reduce the melting point of norcamphor significantly. We cannot exclude the presence of small amounts of melt in our system, due to the high homologous temperature of our experiments and humidity in the air during sample preparation. In fact, the local occurrence of transparent fronts, migrating between sample and glass plates suggest the presence of very thin melt films that may also occur along grain boundaries. However, melt films between grain boundaries are too thin to be optically recognized and can therefore account only for very small volume fractions of melt.

(V) Chemical impurities could be present in the original synthetic starting material (purity degree of 98–99%). As shown by experiments and theoretical considerations, also they can influence grain boundary migration (e.g. Freund et al. 2001; Nakamura et al. 2005; Shvindlerman and Gottstein 2005).

(VI) Several authors demonstrate an effect of crystallographic misorientations on grain growth (Stöckhert and Duyster 1999; Kruhl 2001; Bestmann and Prior 2003; Wheeler et al. 2003). Transferred to our rock analogue system, such misorientations would induce differences in grain boundary velocity and can therefore also impose a relative dragging effect.

(VII) Piazolo et al. (2005) on quartz and Piazolo et al. (2006) on rocksalt demonstrated that the misorientation at grain triple junctions influences grain boundary migration (see also Pande and Masumura 2005; Shvindlerman and Gottstein 2005; Gottstein et al. 2006). Indeed, a stabilization of some triple junctions occurs in our experiments, although no second phases were present in the close vicinity. In the case of nominally pure monocrystalline aggregates, Shvindlerman and Gottstein (2005) suggest that triple junctions most effectively drag grain boundaries.

At the present stage, we are not able to judge which ones and to what extent the aforementioned points II–VII contribute to pinning in our pure and impure experiments. However, we can clearly state that any pinning induced by the glass beads (I) is much more intense, as can be inferred from the dependence of the average grain size on the glass bead volume fraction (Figs. 1, 2). In the context of this study, pinning by solid second phases is therefore more important in case of impure samples than any of the aforementioned alternative pinning regimes.

Static grain growth in second phase affected aggregates: an attempt of a quantitative empirical description

The goal of a grain growth law in general is the prediction of the evolution of grain sizes in a rock either at constant T or as a function of a T–t path. Solely based on Eq. 1 this goal cannot be achieved in the case of polymineralic aggregates. The contribution of all influencing parameters on grain growth should be considered including the spatially resolved microstructural variations (e.g. second phases, crystallographic misfit, grain boundary curvature, chemical impurities) in an appropriate micro-physically based theoretical model. At the present stage, however, for many of these parameters the individual contribution to retardation of grain boundary migration is unknown, requiring more research into these directions in the future. As the effect of the second phases is so dominant in our study, we will confine our considerations on the influence of the second phases on grain growth. Furthermore, we restrict to the behaviour of the bulk aggregate. In this way, local deviations in grain boundary migration velocities, as demonstrated in Fig. 6d, are not considered, as they are averaged out over the entire aggregate. Since normal grain growth is retarded by the presence of second phases in the experiments, Eq. 1 is limited in its applicability and has to be converted in order to predict the evolution of a matrix grain size for different second-phase contents. Particularly, the effect of Zener pinning has to be integrated into the grain growth law. For this purpose, the growth exponent n and the growth constant k were calculated in a first step for stage II of each experiment individually by a least square regression of the $(D^n - D_0^n)$ over $(t - t_0)$ data space (Fig. 2 of electronic supplementary material). The fact that n changes as a function of second-phase grain size and volume fraction requires the integration of these parameters into Eq. 1. In a second step, the mean values of the stage IV data points were calculated to obtain the finally stabilized grain sizes for the corresponding experiments. Note that the aforementioned abnormal deviation of grain sizes of experiment X10 is clearly visible in Fig. 2 of electronic supplementary material. They have smaller values than in the case for grain sizes of volume fractions of 0.16.

Regression lines for mean n and k values were fitted for stages II and IV for each experiment in a last, third step. Due to the time dependence and independence of grain size D in stages II and IV, respectively, Eqs. 5 and 6 are necessary to define the two regression lines. Consequently, two different constants k' and k'' are required.

$$D^n - D_0^n = k' \cdot \Delta t \quad (5)$$

$$D^n - D_0^n = k'' \quad (6)$$

The intersection of the regression line of stages II and IV defines the point, where a transition from constant grain growth to grain size stabilization occurs. The onset of stage IV as well as the transition between stages II and IV depend on the volume fraction of the second phases, as seen from the shifted intersection point in x-direction with decreasing f_p.

A closer look on the transition points between stages II and IV (Fig. 3 of electronic supplementary material) reveals that for higher f_p the transition point is extended into a transition zone, whose width increases with increasing f_p. This transition zone, which is identical to stage III of Andrade and Aboav (1966), correlates directly with an enhanced probability for a migrating grain boundary to become finally immobilized by the smaller inter-particle distance of the second phases with increasing f_p. The immobilization occurs not abruptly but rather during a time interval characterized by an increasing number of pinned grain boundaries, which is related to statistical variations in the interparticle spacing of second phases and cluster sizes. Especially, large clusters will affect the final stabilization of a grain boundary earlier than small clusters or individual second phases, an effect which becomes more pronounced with increasing f_p. Note that in the following the transition between stages II and IV will be treated as a single spot (intersection point). This simplification is justified because the transition mostly covers a short time interval compared to the entire grain growth history, and the deviation in grain size compared to a continuous growth behaviour is limited only.

Comparable to the trend lines for stage II, the calculated individual growth exponent n decreases from around 4.6 ($f_p = 0.008$ and 0.017) to 2.9 ($f_p = 0.33$) and the constant k' from 2.87E + 11 ($f_p = 0.008$ and 0.017) to 5.27E + 05 ($f_p = 0.33$) with increasing second-phase content (Fig. 8). The n-values are typical values of 2–5 as observed in other studies depending on the activated rate limiting process (Brook 1976; Covey-Crump 1997; Evans et al. 2001). Based on numerical models, however, the relationship between n and the second-phase volume fraction is contradictory. Faul and Scott (2006), for example, obtain n-values of 4 for their partially molten monomineralic olivine aggregates. While Srolovitz et al. (1984) found no dependence of the grain growth exponent on the amount of second phases, El-Khozondar et al. (2006) demonstrated an increase in n with increasing second-phase content. In their study, however, matrix as well as second phases could grow, which differs from our experimental setup. In our experiments, the decrease in n with increasing second-

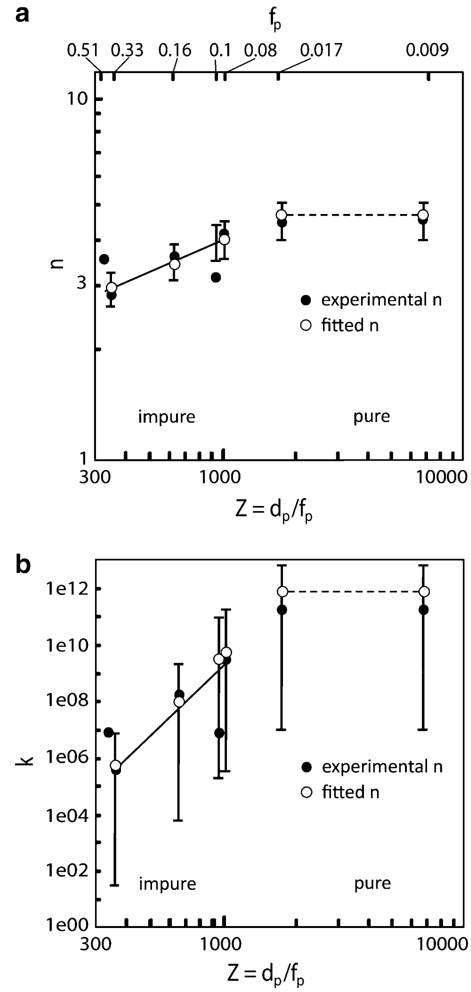

Fig. 8 Dependence of n and k on the Zener parameter Z. Both, n (**a**) and k (**b**) show an increase with Z and, therefore, a strong dependence on the second-phase particle size and volume fraction. *Error bars* result from minimum and maximum values of n and k

phase volume fraction might be related to the enhanced number of norcamphor-glass bead interfaces. Consequently, due to a broader grain boundary width between norcamphor–second phase compared to norcamphor–norcamphor, the grain boundary volume increases with increasing glass bead content. Hence, the flux via intergranular diffusion might be higher due to an enhanced grain boundary porosity eventually allowing even larger molecules to be transported along the interfaces, which in turn enhances the grain growth.

The aforementioned dependence of the calculated individual n and k values on the volume fraction f_p and size of second phases d_p, i.e. on the Zener parameter Z, is displayed in Fig. 8. These relationships can be mathematically expressed by two power laws:

$$n = a_n \cdot Z^{b_n} \quad (7)$$

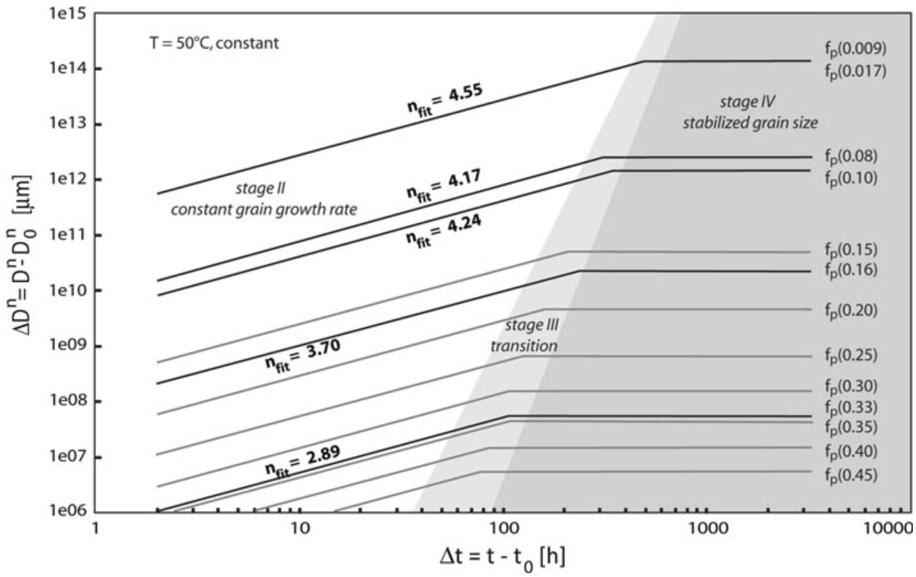

Fig. 9 Quantitative empirical description of the grain size evolution for a two-phase system. The model (*grey lines*) is calibrated for a two-phase system consisting of norcamphor and micro glass-beads, and $0.08 \geq f_p \leq 0.5$. For smaller f_p, this system is not affected by Zener pinning anymore (cf. Fig. 7). *Black lines* refer to the fitted experiment data

$$k = a_k \cdot Z^{b_k} \tag{8}$$

with a_n and a_k as constants, and b_n and b_k describing the slopes of the graphs in Fig. 8, relating to n and k, respectively.

With regard of this dependence, the classical grain growth law (Eq. 1) can be adapted by substituting n and k with Eqs. 7 and 8. The new grain growth law includes the influence of second phases by incorporating the effect of Zener pinning:

$$D^{a_n \cdot Z^{b_n}} - D_0^{a_n \cdot Z^{b_n}} = a_k \cdot Z^{b_k}(t - t_0) \tag{9}$$

By substituting a_k and b_k with the specific $a_{k'}$ and $b_{k'}$, and $a_{k''}$ and $b_{k''}$ for stages II and IV, respectively, Eq. 9 can now be used to predict the changes in matrix grain size with time for different volume fractions and sizes of second phases. This procedure allows the construction of a time-integrated grain size evolution map for a two-phase aggregate (Fig. 9).

Relevance for nature and conclusions

Based on the continuous monitoring of the microstructural evolution in our experiments, a discrimination of different pinning regimes is possible. Their effect on the pinning of the matrix grain size depends on the volume fraction, size and dispersion of the second-phase particles as well as on the size of the matrix grains relative to the interparticle distances. Comparing the experimentally obtained microstructures with those from contact metamorphic polymineralic marbles form the Calcare di Angolo (Adamello pluton, Italy, see Brodhag 2009) indicates identical pinning behaviour. Figure 10 shows two samples close to the pluton's contact, which have seen peak metamorphic temperatures of 595 and 630°C. MPP (Fig. 10a) as well as CPP (Fig. 10b) can both be recognized. For similar grain sizes of the second phases, the calcite grain size decreases with increasing f_p, which correlates in an excellent manner with the experiments (compare Figs. 2 and 10). Additionally, we have a transition from MPP to CPP with increasing f_p. Despite the fact that nature is subjected to complex *P*–*T*–*t* paths, the correlation between natural and experimental microstructures indicates that the pinning processes detected in our experiments are relevant in polymineralic natural rocks undergoing elevated metamorphic conditions. Particularly, the effect of changing *T*–*t* conditions during grain growth needs special attention in future experimental studies.

Based on our experiments it becomes also evident that despite constant bulk growth rates, the grain boundary velocities can vary dramatically on the local scale (Fig. 6). In nature, this has important consequences for the interpretation of grain internal 'mineral inclusions' or 'cores' (Jessell et al. 2003). In the case of a formerly pinned and then released grain boundaries, such grain internal features can be trapped quite rapidly. In this way, also very rapid local growth behaviour of the matrix phase might be stored in polymineralic rocks potentially allowing analyses for highly resolved time information, when studying such inclusion–overgrowth relationships on a statistical base in natural rocks.

Our experiments further suggest that stabilized grain sizes evolve, provided that enough time for grain growth at elevated temperatures was available. This point applies well to nature in the case of regional metamorphic rocks (see discussion in Herwegh et al. 2005) but might be debatable for contact metamorphic rocks with relatively

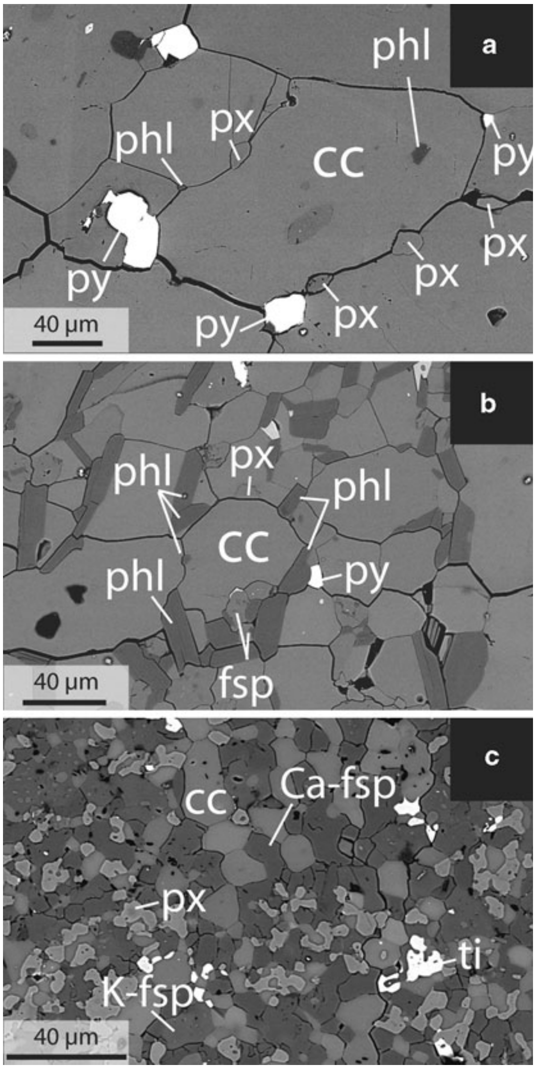

Fig. 10 Backscatter electron images from contact metamorphic polymineralic marbles from the Calcare di Anglo (Adamello contact aureole, Italy), showing pinning processes of calcite grain boundaries identical with those found in the norcamphor experiments. Note the increasing grain size of calcite with decreasing second-phase content (bottom up). **a** Large calcite grain (cc) affected by multiple particle pinning (MPP) by at least eight-second-phase particles (sample SB05-09: peak metamorphic temperature 595°C, 0.1 second-phase volume fraction). Compare with microstructures of experiments X10 and X16 of Fig. 2b. **b** Clustered particle pinning (CPP) controls the intermediate size of calcite grain (cc), (sample SB05-09: peak metamorphic temperature 595°C, 0.3 second-phase volume fraction). Compare with microstructures of experiment X33 of Fig. 2b). **c** High second-phase content completely pins the calcite grain boundaries resulting in small calcite grain sizes (sample SB05-07: peak metamorphic temperature 630°C, 0.6 second-phase volume fraction). Compare with microstructures of experiment X51 of Fig. 2. Second phases are pyroxene (*px*), pyrite (*py*), phlogopite (*phl*), feldspar (*fsp*) and titanite (*ti*); for more detail see Brodhag (2009)

short-lived peak metamorphic conditions. In any case, the maximum grain size reached does closely depend on the dominant pinning regimes. In case of CPP or MPP, for example, much smaller final grain sizes will result compared to SPP or TJP. Equation 9 and the resulting model for grain size evolution (Fig. 9) provide an attempt of a description for the growth of a matrix phase as function of time and different second-phase volume fractions at constant temperature. Owing to the facts that identical pinning processes occur in nature and experiment and the common appearance of Zener pinning in polymineralic rocks (Berger and Herwegh 2004; Ohuchi and Nakamura 2007a, b), our approach can be transferred to natural systems. Nevertheless, at the present stage Eq. 9 has the following restrictions: (1) It is calibrated for a two-phase system consisting of norcamphor and glass beads allowing only the matrix phase to grow while the grain size of the second phase remains fixed. In comparison to nature, a system with a fixed grain size for the second phase is only realistic for fast-growing matrix grains and slowly growing second phases. In all other situations, also the second phase will grow requiring considerations on coupled grain growth (Solomatov et al. 2002; Herwegh et al. 2005). (2) With a homologous temperature of about 0.88, our experiments were driven at relatively high temperature. In nature, lower temperatures and the presence of fluid-affected mass-transport properties along grain boundaries have to be considered, which will affect the grain boundary mobility and, therefore, the pinning capabilities of second phases. (3) The performance of the experiments at constant temperature prevents information on the temperature dependence of the involved pinning and grain growth processes. The activation terms, however, could be integrated in Eq. 9 with an additional experimental suite performed at different temperatures. (4) The spherical shape of the second phases represents a further simplification. Many minerals are either rod-shaped (pyroxenes, amphiboles) or platy (sheet silicates). Their shape will affect the pinning behaviour and, therefore, also influence Eq. 9 (Nes et al. 1985). (5) So far, our approach is only valid for a homogeneous dispersion of the second phases and cluster sizes not larger than 131.6 µm. Agglomeration of second phases in larger clusters or even bands cannot satisfyingly be treated. (6) Finally, mineral stabilities change in *T–t* space and so will the mineral assemblage in polymineralic rocks. Nucleation of new phases can dramatically affect the pinning behaviour at a specific temperature interval by changing not only the mineralogy of the second phases but also their size, volume fraction and dispersion (for more details see Brodhag 2009 and Brodhag et al., in review). Although the pinning processes observed in our study will also hold for these situations, our model does not take into account such phase changes. Furthermore, mineral reactions between second phases and matrix phase will further limit our approach. Despite these restrictions the good news is that all these effects could be integrated in mathematical formulations like Eq. 9 by using appropriate

HT–HP experimental approaches on real rocks and/or calibrations of well-documented natural rock suites, which underwent contact metamorphism under well-defined *P–T–t* paths. In this sense, the present study provides a first attempt for a new research direction in the field of metamorphic petrology and structural geology leaving a great potential for future studies.

Acknowledgments We would like to thank Ralph Mettier for writing the Matlab routine for iterative fitting of n and k values of our experimental data, Andreas Ebert for proofreading and discussion, as well as Robyn Pickering for proofreading. M. Bestmann, M. Jessell, J.H.P. de Bresser and an anonymous reviewer are acknowledged for their constructive reviews, which helped to improve the manuscript significantly. Financial support by SNF by project grants numbers 200021-105316 and 200020-117514 is acknowledged.

References

Andersen I, Grong O (1994) Analytical modelling of grain growth in metals and alloys in the presence of growing and dissolving precipitates—1. Normal grain growth. Acta Metall Mater 43(7):2673–2688

Andrade ENDC, Aboav DA (1966) Grain growth in metals of close-packed hexagonal structure. Proc R Soc Lond A Math Phys Sci 291(1424):18–40

Bauer P, Palm S, Handy MR (2000a) Strain localization and fluid pathways in mylonite: inferences from in situ deformation of a water-bearing quartz analogue (norcamphor). Tectonophysics 320(2):141–165

Bauer P, Rosenberg C, Handy MR (2000b) 'See-through' deformation experiments on brittle-viscous norcamphor at controlled temperature, strain rate and applied confining pressure. J Struct Geol 22:281–289

Becker JK, Bons PD, Jessell MW (2008) A new front-tracking method to model anisotropic grain and phase boundary motion in rocks. Comput Geosci 34:201–212

Berger A, Herwegh M (2004) Grain coarsening in contact metamorphic carbonates: effects of second-phase particles, fluid flow and thermal perturbations. J Metamorph Geol 22:459–474

Bestmann M, Prior DJ (2003) Intragranular dynamic recrystallization in naturally deformed calcite marbles: diffusion accommodated grain boundary sliding as a result of subgrain rotation recrystallization. J Struct Geol 25:1597–1613

Bestmann M, Piazolo S, Spiers CJ, Prior DJ (2005) Microstructural evolution during initial stages of static recovery and recrystallization: new insights from in situ heating experiments combined with electron backscatter diffraction analysis. J Struct Geol 27:447–457

Bons PD (1993) Experimental deformation of polyphase rock analogues, vol 110. Universiteit Utrecht, Utrecht, p 207

Bons PD, Jessell MW, Evans L, Barr T, Stüwe K (2000) Modelling of anisotropic grain growth in minerals. In: Koyi HA, Mancktelow NS (eds) Tectonic modeling: a volume in honor of Hans Ramberg. Geological Society of America Memoir 193, Boulder, pp 45–49

Brodhag SH (2009) Static grain growth in polyphase systems—insights from nature and experiments. Unpublished Ph.D. thesis, University of Bern, Bern, 133 pp

Brook RJ (1976) Controlled grain growth, vol 9. Academic, New York, pp 331–364

Burhan N, Ferry M (2006) Changes in grain size distribution of a submicron grained Al–Sc alloy during high temperature annealing. Mater Sci Forum 519–521:1617–1623

Carlson WD, Gordon CL (2004) Effects of matrix grain size on the kinetics of intergranular diffusion. J Metamorph Geol 22:733–742

Covey-Crump SJ (1996) The high temperature static recovery and recrystallization behaviour of cold-worked Carrara marble. J Struct Geol 19(2):225–241

Covey-Crump SJ (1997) The normal grain growth behaviour of nominally pure calcitic aggregates. Contrib Mineral Petrol 129:239–254

Covey-Crump SJ, Rutter EH (1989) Thermally-induced grain growth of calcite marbles on Naxos Island, Greece. Contrib Mineral Petrol 101:69–89

Dai SL, Delplanque J-P, Lavernia EJ (1999) Effect of secondary phase particles on postrecrystallization grain growth in reactive spray deposited 5083 Al alloys. J Mater Res 14(7):2814–2823

Dresen G, Wang Z, Bai Q (1996) Kinetics of grain growth in anorthite. Tectonophysics 258:251–262

Ebert A, Herwegh M, Evans B, Pfiffner OA, Austin N, Vennemann T (2007) Microfabrics in carbonate mylonites along a large-scale shear zone (Helvetic Alps). Tectonophysics 444:1–26

El-Khozondar R, El-Khozondar H, Gottstein G, Rollet A (2006) Microstructural simulation of grain growth in two-phase polycrystalline materials. Egypt J Solids 29(1):35–47

Evans B, Renner J, Hirth G (2001) A few remarks on the kinetics of static grain growth in rocks. Int J Earth Sci 90:88–103

Faul UH, Scott D (2006) Grain growth in partially molten olivine aggregates. Contrib Mineral Petrol 151:101–111

Ferry M, Hamilton NE, Humphreys FJ (2005) Continuous and discontinuous grain coarsening in a fine-grained particle-containing Al–Sc alloy. Acta Mater 53:1097–1109

Freund D, Rybacki E, Dresen G (2001) Effect of impurities on grain growth in synthetic calcite aggregates. Phys Chem Miner 28:737–745

Fueten F (1997) A computer-controlled rotating polarizer stage for the petrographic microscope. Comput Geosci 23(2):203–208

Fueten F, Hynes K, Van Luttikhuisen R (2002) An experimental setup for the analysis of analogue deformation experiments using the rotating polarizer stage. J Struct Geol 24:241–245

Goodchild J, Fueten F (1998) Edge detection in petrographic images using the rotating polarizer stage. Comput Geosci 24(8):745–751

Gottstein G, Molodov DA, Shvindlerman LS (2006) Kinematics, dynamics, and microstructural effects of grain boundary junctions. J Mater Sci 41:7730–7740

Haggert K, Cox SDJ, Jessell MW (1992) Observation of fault gouge development in laboratory see-through experiments. Tectonophysics 204:123–136

Hazzledine PM, Oldershaw RDJ (1990) Computer simulation of Zener pinning. Philos Mag A 61(4):579–589

Herwegh M, Berger A (2003) Differences in grain growth of calcite: a field-based modeling approach. Contrib Mineral Petrol 145:600–611

Herwegh M, Berger A (2004) Deformation mechanisms in second-phase affected microstructures and their energy balance. J Struct Geol 26:1483–1498

Herwegh M, Handy MR (1996) The evolution of high temperature mylonitic microfabrics: evidence from simple shearing of a quartz analogue (norcamphor). J Struct Geol 18:689–710

Herwegh M, Handy MR (1998) The origin of shape preferred orientation in mylonite: inferences from in situ experiments on polycrystalline norcamphor. J Struct Geol 20(6):681–694

Herwegh M, Kunze K (2002) The influence of nano-scale second-phase particles on deformation of fine grained calcite mylonites. J Struct Geol 24:1463–1478

Herwegh M, Handy MR, Heilbronner R (1997) Temperature and strain rate dependent microfabric evolution in monomineralic mylonite: evidence from in situ deformation of a rock analogue. Tectonophysics 280:83–106

Hillert M (1965) On the theory of normal and abnormal grain growth. Acta Metall 13:227–238

Jessell MW, Bons PD, Evans L, Barr T, Stüwe K (2001) Elle: the numerical simulation of metamorphic and deformation microstructures. Comput Geosci 27:17–30

Jessell MW, Kostenko O, Jamtveit B (2003) The preservation potential of microstructures during static grain growth. J Metamorph Geol 21:481–491

Joesten RLJ (1991) Kinetics of coarsening and diffusion-controlled mineral growth. In: Kerrick DM (ed) Contact metamorphism. Reviews in mineralogy. Mineralogical Society of America, Washington, pp 507–582

Kad BK, Hazzledine PM (1997) Monte Carlo simulations of grain growth and Zener pinning. Mater Sci Eng A238:70–77

Karato S (1989) Grain growth kinetics in olivine aggregates. Tectonophysics 168:255–273

Kruhl JH (2001) Crystallographic control on the development of foam textures in quartz, plagioclase and analogue material. Int J Earth Sci 90:104–117

Manohar PA, Ferry M, Chandra T (1998) Five decades of the Zener equation. ISIJ Int 38(9):913–924

Mas DL, Crowley PD (1996) The effect of second-phase particles on stable grain size in regionally metamorphosed polyphase calcite marbles. J Metamorph Geol 14:155–162

Means WD (1983) Microstructure and micromotion in recrystallization flow of octachloropropane: a first look. Int J Earth Sci 72(2):511–528

Miodownik MA (2005) Grain boundary engineering with particles. Scr Mater 54:993–997

Moelans N, Blanpain B, Wollants P (2005) A phase field model for the simulation of grain growth in materials containing finely dispersed incoherent second-phase particles. Acta Mater 53:1771–1781

Moelans M, Blanpain B, Wollants P (2006) Phase field simulations of grain growth in two-dimensional systems containing finely dispersed second-phase particles. Acta Mater 54:1175–1184

Nakamura M, Yurimoto H, Watson EB (2005) Grain growth control of isotope exchange between rocks and fluids. Geology 33(10):829–832

Nam TN, Otoh S, Masuda T (1999) In situ annealing experiments of octachloropropane as a rock analogue: kinetics and energetics of grain growth. Tectonophysics 304:57–70

Nes E, Ryum N, Hunderi O (1985) On the Zener drag. Acta Metall 33(1):11–22

Nollet S, Hilgers C, Urai JL (2006) Experimental study of polycrystal growth from an advecting supersaturated fluid in a model fracture. Geofluids 6:185–200

Ohuchi T, Nakamura M (2006) Microstructure evolution of aqueous fluid-bearing wehrlites: implications for the fluid distribution in polymineralic rocks. J Geophys Res 111:B01201

Ohuchi T, Nakamura M (2007a) Grain growth in the forsterite–diopside system. Phys Earth Planet Inter 160(1):1–21

Ohuchi T, Nakamura M (2007b) Grain growth in the system forsterite–diopside–water. Phys Earth Planet Inter 161(3–4):281–304

Olgaard DL, Evans B (1986) Effect of second-phase particles on grain growth in calcite. J Am Ceram Soc 69(11):C272–C277

Olgaard DL, Evans B (1988) Grain growth in synthetic marbles with added mica and water. Contrib Mineral Petrol 100:146–260

Olgaard DL, Fitz Gerald JD (1993) Evolution of pore microstructures during healing of grain boundaries in synthetic calcite rocks. Contrib Mineral Petrol 115:138–154

Pande CS, Masumura RA (2005) Grain growth and deformation in nanocrystalline materials. Mater Sci Eng A 409:125–130

Park Y, Ree J-H, Kim S (2001) Lattice preferred orientation in deformed-then-annealed material: observations from experimental and natural polycrystalline aggregates. Int J Earth Sci 90:127–135

Petrishcheva E, Renner J (2005) Two-dimensional analysis of pore drag and drop. Acta Mater 53:2793–2803

Piazolo S, Prior DJ, Holness MD (2005) The use of combined cathodoluminescence and EBSD analysis: a case study investigating grain boundary migration mechanisms in quartz. J Microsc 217(2):152–161

Piazolo S, Bestmann M, Prior DJ, Spiers CJ (2006) Temperature dependent grain boundary migration in deformed-then-annealed material: observations from experimentally deformed synthetic rocksalt. Tectonophysics 427:55–71

Poirier J-P, Guillopé M (1979) Deformation induced recrystallization of minerals. Bull Minéral 102:67–74

Renner J, Evans B, Hirth G (2001) Grain growth and inclusion formation in partially molten carbonate rocks. Contrib Mineral Petrol 142(5):501–514

Rios PR, Gottstein G, Shvindleman LS (2002) An irreversible thermodynamic approach to normal grain growth with a pinning force. Mater Sci Eng A332:231–235

Rosenberg CL, Handy MR (2000) Syntectonic melt pathways during simple shearing of a partially molten rock analogue (norcamphor–benzamide). J Geophys Res 105(B2):3135–3149

Rosenberg CL, Handy MR (2001) Mechanisms and orientation of melt segregation paths during pure shearing of a partially molten rock analog (norcamphor–benzamide). J Struct Geol 23:1917–1932

Schenk O, Urai JL, Evans B (2005) The effect of water on recrystallization behavior and grain boundary morphology in calcite-observations of natural marble mylonites. J Struct Geol 27:1856–1872

Schenk O, Urai JL, Piazolo S (2006) Structure of grain boundaries in wet, synthetic polycrystalline, statically recrystallizing halite—evidence from cryo-SEM observation. Geofluids 6:93–104

Shvindlerman LS, Gottstein G (2005) Cornerstones of grain structure evolution and stability: vacancies, boundaries, triple junctions. J Mater Sci 40:819–839

Simpson CJ, Aust KT, Winegard WC (1971) The four stages of grain growth. Metall Trans 2:987–991

Smith CS (1948) Grains, phases, and interfaces: an interpretation of microstructure. Trans AIME 175:15–51

Solomatov VS, El-Khozondar R, Tikare V (2002) Grain size in the lower mantle: constraints from numerical modeling of grain growth in two-phase systems. Phys Earth Planet Inter 129:265–282

Srolovitz DJ, Anderson MP, Grest GS, Sahni PS (1984) Computer simulation of grain growth-III. Influence of a particle dispersion. Acta Mater 32(9):1429–1438

Stöckhert B, Duyster J (1999) Discontinuous grain growth in recrystallised vein quartz—implications for grain boundary structure, grain boundary mobility, crystallographic preferred orientation, and stress history. J Struct Geol 21:1477–1490

Streit JE, Cox SF (2002) Evolution of fracture networks in shear zones: insights from see-through experiments on biphenyl aggregates. J Struct Geol 24:107–122

Tullis J, Yund RA (1982) Grain growth kinetics of quartz and calcite aggregates. J Geol 90:301–318

Urai JL, Means WD, Lister GS (1986) Dynamic recrystallization of minerals. Mineral and rock deformation: laboratory studies—The Patterson volume. American Geophysical Union, Geophysical Monograph 36, Washington, pp 161–199

Walte NP, Bons PD, Passchier CW (2005) Deformation of melt-bearing systems—insight from in situ grain-scale analogue experiments. J Struct Geol 27:1666–1679

Walte NP, Becker JK, Bons PD, Rubie DC, Frost DJ (2007) Liquid-distribution and attainment of textural equilibrium in a partially-molten crystalline system with a high-dihedral-angle liquid phase. Earth Planet Sci Lett 262:517–532

Weygand D, Bréchet Y, Lépinoux J (2000) Inhibition of grain growth by particle distribution: effect of spatial heterogeneities and of particle strength dispersion. Mater Sci Eng A 292:34–39

Wheeler J, Jiang Z, Prior DJ, Tullis J, Drury MR, Trimby PW (2003) From geometry to dynamics of microstructure: using boundary lengths to quantify boundary misorientations and anisotropy. Tectonophysics 376:19–35

Zheng YG, Lu C, Mai Y-W, Zhang HW, Chen Z (2006) Model-based simulation of normal grain growth in a two-phase nanostructured system. Sci Technol Adv Mater 7:812–818